Metal nanoparticles (NPs) in photocatalysis: advances and challenges

Houssein Nasrallah, Fatima Douma, Houeida Issa Hamoud, Mohamad El-Roz

Metal nanoparticles (NPs) in photocatalysis: advances and challenges

Houssein Nasrallah, Fatima Douma, Houeida Issa Hamoud and Mohamad El-Roz*

Normandie Université, ENSICAEN, UNICAEN, CNRS, Laboratoire Catalyse et Spectrochimie, 14000 Caen, France.

*Corresponding author. E-mail addresses: mohamad.elroz@ensicaen.fr

Table of Contents

Abstract

Metal nanoparticles (MNPs) are widely used in photocatalysis as plasmonic photocatalyst or as cocatalyst supported on semiconductor photocatalysts. They play a crucial role in the adsorption and the activation processes of the reactants and the intermediates as well as in the separation of the generated electrons/holes charges. In this chapter we highlight the utility of the MNPs in various photocatalytic processes. First, we report and discuss the optical and electronic behaviors of the MNPs and how these properties make them promising in photocatalysis. Then, we discuss their different roles in photocatalytic, water splitting, CO_2 reduction and green chemistry.

Keywords*:* Metal Nanoparticles, Photocatalysis, Plasmon, Photon's Energy, Green Chemistry

1. Metal nanoparticles (MNPs): Definition and applications

Metallic nanoparticles (MNPs) with the size range of 1-100 nm have attracted much attention because of their unique shape and size-dependent chemical and physical properties that differ from their bulk counterparts. Their first application goes back to antiquities where gold and silver NPs have been embedded in the stained-glass windows to make brilliant colors (Hunt, 1976) such as the synthesis of purple of Cassis by the reaction between gold trichloride ($AuCl_3$) and Tin (Sn) as well as the heat treatment of gold powder with potassium silicate to obtain a red colored glass (Wisniak et al., 2009). Currently, metal nanoparticles are used in different domains such as sensors manufacturing (Liu et al., 2010), biomedicine (Fu et al., 2018; Venkatesh et al., 2018), optoelectronics (Wang et al., 2016) and solar cell manufacturing (Arinze et al., 2016). But, of the

highly advanced applications of MNPs are found in catalysis despite their noted limitations in this domain (Zhou et al., 2018).

Nowadays, the use of metal nanoparticles NPs as photocatalyst or co-catalyst to convert green and free light energy (solar light) into chemical energy is attracting much more attention (Han et al., 2018; Liu et al., 2017 and Xiao et al., 2014). This is mainly due to the unique electronic and optical behaviors of MNPs which depend of their nature, morphology and size as we will see later in this chapter.

2. Electronic and optical behavior of metal nanoparticles

2.1. Local Surface Plasmonic Resonance (LSPR)

The Local Surface Plasmonic Resonance refers to the collective oscillations of electrons at the interface of metal nanoparticles (NPs), which is produced through the interaction of metal NPs with incident light with specific wavelength. The resulted LSPR frequency can be easily measured by UV–Visible spectroscopy. For example, the UV–Visible absorbance spectra of spherical Cu, Au, and Ag NPs with diameters of 20 nm exhibit LSPR absorption bands with wavelength maxima at 580, 530, and 400 nm respectively (Liu et al., 2017). The LSPR of MNPs can be tuned by controlling its size and shape as well as the inter-NPs distance (Huang et al., 2006). In general, a red shift of the LSPR frequency is observed by increasing the corner sharpness of the NPs. This shift is caused by the accumulation of surface charges at the crystal corners leading to a better charge separation (Wiley et al., 2007). Increasing the NP size also red-shifts the LSPR frequency to the longer wavelengths. For example, the LSPR absorption peaks of gold nanorods shift from visible to the near infrared range by increasing the size ratio of gold nanorods from 2.4 to 5.5 nm (Wiley et al., 2007).

The oscillating electrons on the MNPs surface stimulated via light-MNPs interaction (called also hot electrons) have a femtoseconds lifetime. Their relaxation is then occurred through three possible pathways:

a) by *elastic radiative reemission* of photons (photoluminescence)

b) via *nonradiative Landau damping* producing a local heating

c) and/or via *interaction of excited surface plasmons with an adsorbate acceptor*.

In general, these phenomena have a significant impact on the efficiency of the NPs when they are used as photocatalysts or co-catalysts.

2.2. Energy transfer of the plasmon

The energy transfer is a general phenomenon that is generally observed between a donor (in general at the excited state) and an acceptor. It occurs via different possible processes depending of the intrinsic properties of the donor and the acceptor. In the case of the energy transfer of the plasmon, the donor is the excited MNPs and the transfer is promoted through different possible pathways:

(1) Elastic radiative reemission of photons: the relaxation of the hot electrons of the MNPs produces a photonic emission at higher wavelength of the excited source (Fig. 1). This emission can be absorbed by the chemisorbed molecules on the NPs surface initiating then a chemical reaction. Generally, this phenomenon requires large-sized particles (> 40 nm for AuNPs) and UV irradiation to achieve the excitation of the internal electronic transition of the adsorbed substrate.

(2) Landau damping phenomenon: gives rise to electron-hole pair generation resulting from interband and intraband transitions. Electron-hole pairs can follow two routes: i) the energetic photo-excited electrons subsequently scatter into unpopulated electronic states of adsorbates which causes chemical bonds destabilization and ii) relaxation through electron-electron collisions and

electron-phonon interaction leading to a local heating. The heat is then transferred to the MNPs environment (reactant molecules and/or to the solution), increasing therefore the local temperature. This photothermal phenomenon can promote a chemical reaction when the thermal energy released is higher than the required barrier energy.

(3) Chemical interface damping (CID): *when* excited surface plasmons interact with unoccupied adsorbate acceptors, they induce a direct electron transfer from the MNPs into the adsorbate. These energy transfer of plasmon is at the origin of the plasmonic photocatalysis where MNPs are used as isolated photocatalysts, as we will see in the "part 3" of this chapter.

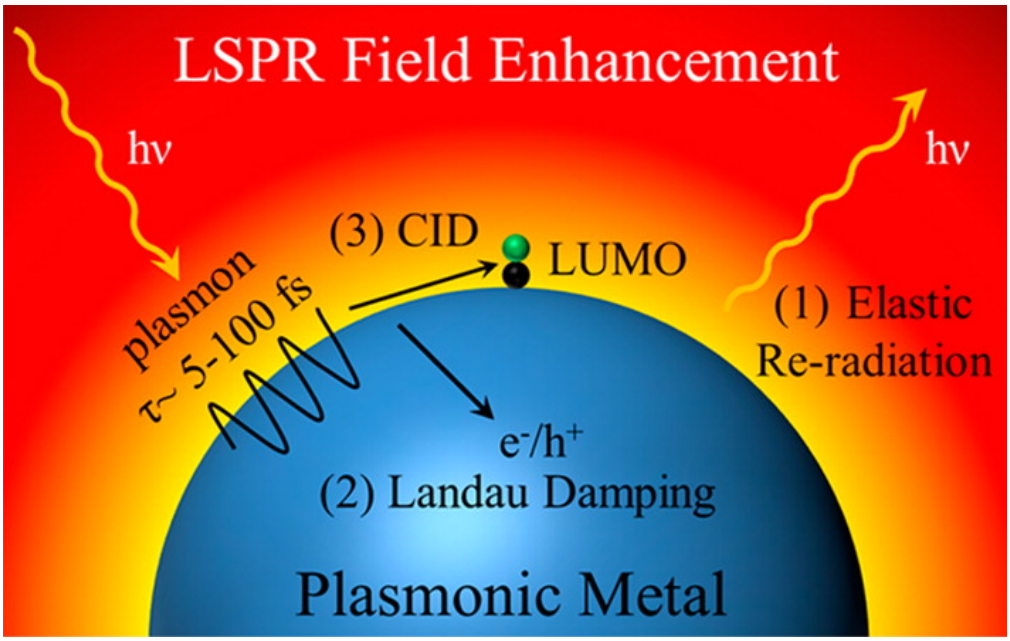

Fig. 1. Scheme showing the three possible dephasing mechanisms of the energy transfer of oscillating surface plasmons. Copyright 2014 American Chemical Society. Reprinted with permission from Kale et al., 2014.

2.3. Local Electric Field (LEF)

In addition to the presented pathways above, local electric field (LEF) is a common phenomenon for NPs. An oscillating electric dipole can be produced by exposure of MNP to an

irradiation near to their plasmon resonance frequency, producing an intense LEF near to the NP's surface. Its intensity can be even up to 1000 times higher than that of the incident electric field. Furthermore, the presence of two or more NPs in a close proximity to each other, the electric field can be significantly more important than that on isolated NPs (Hao et al., 2004). For example, the increase of Ag nanocube inter-distances induces an enhancement of the electric field which promotes the electron-hole pair generation rate (Linic et al., 2011). This phenomenon has a significant impact on photocatalytic reaction by sub-exciting the hot electron generated at the interface of a semiconductor/MNPs.

3. Fundamental aspect of the use of MNPs in photocatalysis:

3.1. Photocatalysis with supported metal NPs on semiconductors: General mechanism

The use of MNPs in photocatalysis has been proposed to overcome some limitations of the semiconductor (SC) photocatalysts, initially discovered by Fujishima et al. in 1972 when a TiO_2 SC was used in electrochemical photolysis of water. When the SC is irradiated with an energy higher than its band gap energy, the electrons can be excited from the valence band (VB) of the SC to its conduction band (CB) resulting the formation of electron-hole pairs (charge carriers). These charges can initiate redox reactions with the adsorbed molecules on the SC surface. However, the SC photocatalysts generally presents some limitations, affecting their quantum efficiency, such as the wide band gap energy (selectively excited by UV light) and/or the fast electron–hole recombination (more than 95%). In this context, the modification of the SC surface by MNPs can enhance considerably the performance of the system. The MNPs is capable to extend the light absorption of the MNPs/SC composite to the visible light range or enhance the separation of the generated charge versus their recombination. E.g. the MNPs supported on the semiconductor

can play the role of an electron-pool by accumulating the generated electrons or holes. This capacity is crucial for a redox reaction that requires a multi- electrons/holes simultaneous transfer. There are different factors governing the interaction between the MNPs and the semiconductor. These factors explain the performance of the MNPs/SC systems in a photocatalytic reaction and are detailed in the following sections:

3.1.1. Schottky barrier and Ohmic contact

The engineering of semiconductors (SCs) by surface grafting of MNPs is one of the promising approaches to promote an efficient charge separation. This is principally related to the formation of a thermodynamic energy barrier at the metal-semiconductor interface, resulting from the equilibrium bended between the Fermi levels of the metal (E_{fM}) and of the semiconductor (E_{fSC}). This equilibrium depends strongly on the values of the electron affinity (χ_{SC}) of the semiconductor and the work function (W). This later corresponds to the required energy for the excitation of an electron from Fermi to the vacuum level. Depending on this, there are two modes of junctions: **Schottky junction (**$W_M > W_{SC}$) (Fig. 2 (a)) and **Ohmic contact (**$W_M < W_{SC}$) (Fig. 2 (b)), where W_M and W_{SC} correspond to the work function of the metal and the semiconductor, respectively. In the case of $W_M > W_{SC}$, for n-Type semiconductor, the electrons from the conduction band CB (with energy equal to E_{CB}) migrate into the metal leaving positively charged holes (h^+) at the valence band VB (with energy equal to E_{VB}) of the semiconductor (Chouhan et al., 2018; Khan et al., 2015). Considering the low charge density on the later (typically $10^{17} cm^{-3}$), the charge carries are transferred not only from the surface but also from the bulk. The flow of the charge carriers at the semiconductor/metal interface decreases and leads to the formation of a depleted layer (charge space layer). Consequently, an electric field is created from the positive depletion layer to the accumulated negative charges at metal surface leading to the formation of a Schottky

barrier (φ_{SB}). For a n-type semiconductor, the energetic height of the Schottky barrier φ_{SB} is given by Schottky-Mott equation that corresponds to the difference between the metal work function W_M and the electron affinity χ_{SC} of the SC: $\varphi_{SB} = W_M - \chi_{SC}$.

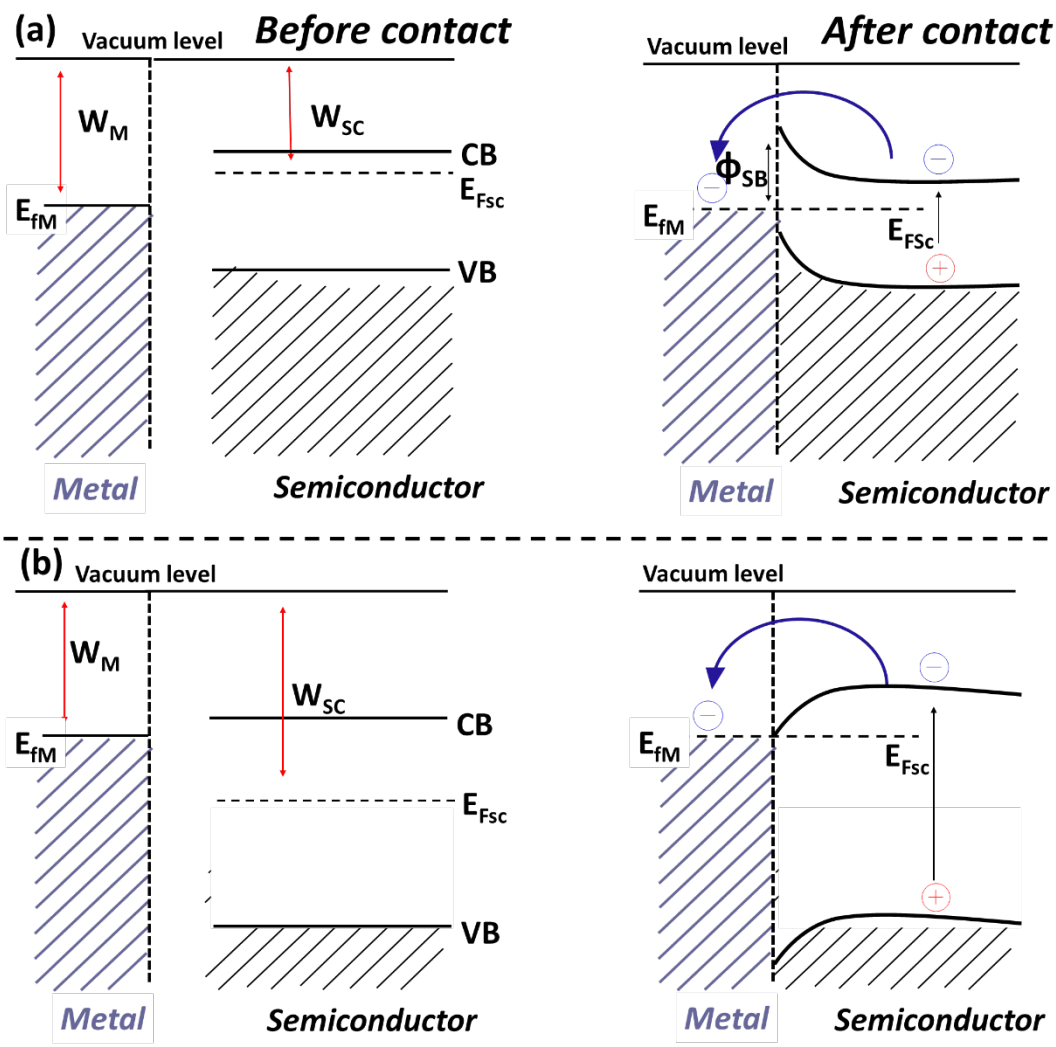

Fig. 2. Energy diagram of supported MNPs on n-Type semiconductor illustrating (a) the Schottky junction and the (b) Ohmic contact.

The formation of the Schottky barrier at the metal-support interface not only acts as an electron trap container, but also promotes the generation of the active sites for reductive reactions,

and thus boosts the properties of MNPs/SC nanocomposite photocatalysts. Generally, the efficiency of the Schottky junction is higher than that of the Ohmic contact in photocatalytic reactions. The absence of a barrier in the case of Ohmic contact promotes the recombination of the charge carriers. The barrier level at the semiconductor-metal interface is strongly affected by the electronegativity and the work function of the metal as well as the nature of the SC.

3.1.2. Quantum tunneling (QT) effect in MNPs/semiconductor composite

As the size of metallic nanoparticles is lowered to sub-nanometer dimensions (d<0.5 nm), an electron tunneling through a conductive junction will be entrenched between them, allowing direct dipolar charge transfer. Quantum tunneling induces obvious modifications in the plasmonic mode, where a mirror-induced bonding dipolar plasmon (MBDP) mode changes to charge transfer plasmon (CTP) mode. Furthermore, QT induces enhancement in the conduction band gap and changes the near and far field properties of the systems, which can be observed by far-field optic and near field spectroscopy (Scholl et al., 2013; Ilawe et al., 2018).

The interparticle spacing is a form of Fowler-Nordheim tunneling by the effect of an external high electric field. The quantum effect results in an electron tunneling from the conduction band of one nanoparticle to the other (Wu et al., 2013). The quantum tunneling effect in plasmonic systems can be affected by the: i) gap thickness; ii) morphological properties of the MNPs; iii) reflective index of the insulating spacer between the MNPs and iv) the wavelength of the incident light. For example, the plasmon tunneling was observed to be negligible at larger resonance wavelengths (Lee et al., 2019).

QT concept can be extended to other plasmonic systems comprising noble metal and semiconductor, in which the hot electrons can migrate from plasmonic NPs to semiconductor CB with much lower energy than that required for over-barrier path.

3.2. Photocatalysis on isolated plasmonic NPs

Despite the tunable and strong interaction between visible light and plasmonic NPs, the photocatalysis on isolated MNPs is not very developed. This is mainly due to the short lifetimes of short lifetimes of plasmon derived charge carriers as well as the rapid quenching of excited adsorbates at metal surfaces (Nitzan, 1981). However, a few interesting direct plasmon driven photocatalysis were reported with high efficiencies. The action mode on these photocatalysts is completely different than that of supported NPs on semiconductor composites and can follow three different pathways (two of them are discussed above in this chapter): i) nonradiative Landau damping (also known as indirect charge transfer); ii) chemical interface damping (CID) with weakly adsorbed substrate (or direct charge transfer) and iii) direct photoexcitation of the hybridized substrate–adsorbate bond. This later is promoted when the reactant is strongly chemisorbed on the metal where the orbitales of molecule are hybridized to form bonding and antibonding state with the metal orbitals. Then the new metal/molecule hybrid state can be activated by a direct photoexcitation causing an electronic transition between hybridized bonding and antibonding states (Kale et al., 2014).

3.3. Photocatalysis on quantum noble metal

Subnanometer metallic clusters constitute a cross-link between the limits of the single atomic and plasmonic NPs, giving rise to interesting electrical, optical and catalytic size-dependent properties. One of the consequences of downsizing the metallic particles to less than the electron wavelength is their quantum molecular dots with distinct energy levels resulting in a sizeable HOMO-LUMO band gap compared to that of SC (Attia et al.; 2017). For example, the hybridization between 4d and 5s in Ag bulk is obviously tuned by the extensive character of 5s electrons in their counterpart in Ag clusters which widens up their band gap energy (Lei et al., 2010). The increase of cluster

size is associated with a narrowing in the band gap. For small metal cluster, the band gap (Eg) is often calculated from the spherical Jellium model (Eg = EF/N1/3), where EF and N are the energy of Fermi level and the number of cluster atoms, respectively (Lin et al., 2009).

In general, metallic clusters show unusual catalytic behavior for heterogeneous based photocatalysis under appropriate irradiation. The high ratio of surface atoms in the clusters facilitates both the interaction with the reactants and the desorption of the products, which increases the kinetics of the photocatalytic reactions. Importantly, the high surface/bulk atomic ratio of cluster is very advantageous to achieve some photocatalytic redox reactions that need multiple electron or hole transfer (e.g., CO_2 reduction or water oxidation). In addition, Metallic clusters are considered to have a significant influence on the charge carrier lifetime by hindering the recombination of photoinduced electron-holes. Nevertheless, the subnano-clusters with multiple active centers cannot be always considered as the most suitable catalyst for a specific product. Thus, the number of atom (surface/bulk ratio) has an important impact on the reactivity of metal co-catalysts because the reaction is controlled by both kinetics and thermodynamics. The metal clusters can play the role of an intermediate relay for an electron transfer between a donor (D) and an acceptor (A) due its redox properties. For large sizes of metal particles, the transfer of electrons to A is not favorable while it can be irreversible in case of few atomic clusters (Belloni et al., 2006). Other limitations of the metal clusters (M) is related to their tendency of migration and aggregation into MNPs with larger size.

3.4. Photocatalysis with non-plasmonic metal NPs

Contrary to the MNPs, visible LSPR band peak can't be observed in case of the non-plasmonic metals such as Pd, Pt, Rh, Ru and Ir. However, they exhibit significant absorption in UV and/or visible light leading to an electron photoexcitation through strong interband transitions

(Smith et al., 2015). These metals are widely used as co-catalysts in many photocatalytic reactions especially in organic synthesis field and H_2 production from water (Davies et al., 2009).

4. Typical applications of MNPs in photocatalysis

4.1. Photocatalytic Water Splitting (WS)

Water splitting to protons and O_2 occurs naturally when the energy of a photon is absorbed by the leaves and converted into chemical energy through a complex photosynthesis process. Artificially, this process is highly endothermic ($\Delta H > 0$) and requires huge amounts of input energy. For this reason, commercial hydrogen gas production results from natural gas or via water electrolysis splitting. Most of the semiconductors with suitable band structures for water splitting are generally active under UV light. Using MNPs/SC system presents a good alternative to overcome this problem and enhance the activity of the SC. The choice of the plasmonic photocatalyst for water splitting depends on several criteria including the electrical/electronic properties, the band gap energy, and the band edge position that must overlap the electrochemical reduction $E°(H^+/H_2)$ and oxidation $E°(O_2/H_2O)$ potentials of water. (Attia et al., 2017; Hisatomi et al., 2015). In a MNPs/SC system, the WS process takes place on both of electron enriched MNPs to reduce H^+ into H_2. This process is generally occurred when an electron transfer from the excited SC, under UV light, to the MNPs takes place (Fig.3). In that case, the water oxidation is promoted by interaction of water with the VB hole of the semiconductor producing O_2 and H^+. The excitation under visible light of the MNPs/SC system could induce another mechanism: the plasmonic hot electron migrates from MNPs to SC CB involving the generation of the H_2 and O_2 on CB and on the MNPs surface, respectively (Fig. 3).

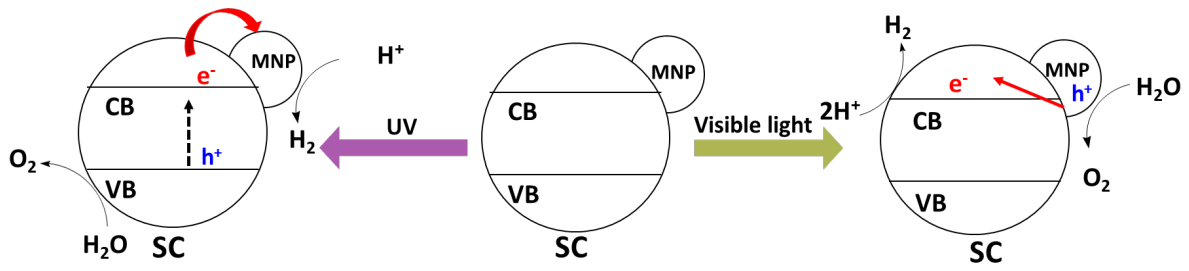

Fig. 3 Photocatalytic Water splitting mechanism under UV irradiation (left) and under visible light (right).

Despite that water oxidation and proton reduction can occur simultaneously in a MNPs/SC photocatalyst system, most of the studies focus on one half of the WS reaction: photocatalytic hydrogen evolution reaction (PHER) or photocatalytic oxygen evolution reaction (POER). In these two-half reactions an electron donor or acceptor are used to compensate the charge. Photoassisted-electrochemical (PEC) water splitting is also investigated using MNPs/SC composite. The choice of the reaction is mainly related to the oxidation vs reduction capacity of the selected systems. In the following sections we summarize some examples used in HER, OER and PEC water splitting using MNPs as plasmonic photocatalysts and/or cocatalysts.

4.1.1. MNPs in photocatalytic hydrogen evolution reaction (PHER)

In general, the H_2 production from water proceeds via H^+ reduction and the oxidation of a sacrificial agent (e.g. methanol, isopropanol, triethanolamine, etc.). Among the noble metals, Pt is reviewed as the best candidate for hydrogen evolution by photocatalytic water splitting owing to: i) its large work function ii) the low Fermi level for photo-generated electron and iii) the special catalytic sites for hydrogen evolution resulted from its good ability to adsorb proton (Hu et al., 2020; Sheng et al., 2013; Shi et al., 2018). When comparing the production of hydrogen in photocatalytic processes, under UV irradiation, using TiO_2 decorated with different MNPs (Pt, Pd, Cu, Ru and Ag), hydrogen production decreased with the following order: Pt-TiO_2>Pd-TiO_2>Cu-

TiO_2>Ru-TiO_2>Ag-TiO_2>TiO_2 (Beasley et al., 2020). A linear relationship between H_2 production and the metal's work function was observed. The reported work function of Pt, Pd, Cu, Ru, and Ag are 5.93, 5.60, 5.10, 4.71, and 4.26 eV, respectively and that of TiO_2 is ranged from 3.8 to 6.0. The work functions of Ru, Cu, and Ag are less than or equal to that of TiO_2 which makes easier the return back of the excited electrons from the metal to TiO_2. This explains their lower activity (Fig. 4). However, higher work function differences (e.g., Pt and Pd) enhance the separation of the photogenerated charges and therefore the performance of the system. This also explain the use of the Pt as counter electrode for photoelectrochemical H_2 production.

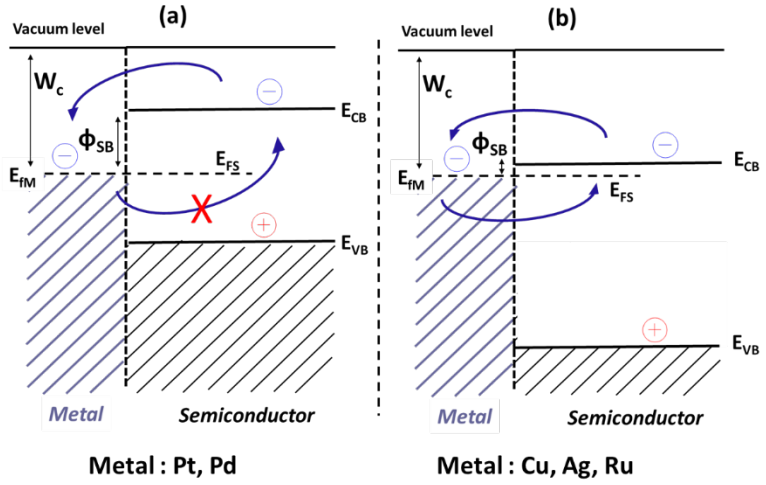

Fig. 4. A schematic illustration of the electron flow under UV irradiation across metal/semiconductor (a) high Schottky barrier, (b) low Schottky barrier interface.

It has been demonstrated that the cationic counterparts $Pt^{\delta+}$ are more suitable for photocatalytic HER due of their lower adsorption ability toward H, comparatively to the deposited metallic Pt NPs. The binding strength between Pt and H atoms could be determined by the electronic density and energy level of the d-orbital for the Pt atom. The electronic density of the d band for the Pt cations is lower than that of metallic Pt clusters, which explain their higher H_2 generation performance. It was also demonstrated that Pt^{4+} ions (embedded in LTA zeolite porous materials)

is more efficient to drive PHER as compared to sample containing selectively Pt^0 NPs. The higher H_2 evolution efficiency was explained by the strong interaction between the isolated water molecules and the ionic Pt dispersed in the cavities of LTA, which provide more efficient electron transfer (Cheng et al., 2018). The metal-H bonding strength is weaker in case of Cu, Ag and Au due to their relatively high occupancy of the anti-bonding hydrogen (1s) and metal (d) states compared to Pt-group metals (Pt, Ru, and Ir). This is also an essential factor for the relatively low performance of the HER of these MNPs. The only limitation of the Pt is its high cost price. Pd could be an excellent alternative to replace platinum for photocatalytic HER owing to their comparable chemical features with large barrier height semiconductor junction in contrast to that of e.g. Au and Ag. Moreover, the price of Palladium is 20% cheaper than the Pt and 50 times more abundant.

It should be noted that one of the challenges when a MNPs is used in photocatalytic hydrogen production is the water formation back reaction that competes with the water splitting process. Interestingly, it was demonstrated that the presence of CO traces on the surface of metallic co-catalysts (Pt, Pd, Rh) might significantly inhibit the reverse reaction of water formation (Wang, 2011). The presence of traces content of iodine ion limits also the water backward reaction by forming a protection layer on Pt NPs surface (Berto et al., 2016; Abe et al., 2003). Furthermore, similar behavior was observed by adding small amount of halogen ions. (Wang et al., 2018).

4.1.2. MNPs in photocatalytic Oxygen Evolution Reaction (POER)

POER is a kinetically challenging and multistep reaction. It requires a considerably large overpotential (1.23 eV Gibbs) coupled with four proton-electron transfers and O-O bond

formation. In a recent study using Kelvin probe force microscopy (KPFM) coupled with element mapping, highlights on the role of the MNPs water oxidation and O_2 formation using Au/TiO_2 as plasmonic photocatalyst model have been reported. It was shown that the difference between the work function of the tip and the sample (contact potential difference (CPD)) was significantly reduced compared to the pure TiO_2. This was attributed to the formation of Schottky interfacial contact between Au and TiO_2 (Moon et al., 2018; Wang et al., 2017). The surface photovoltage (SPV) profile proves that the plasmonic holes are mainly localized around Au/TiO_2 interface. Therefore, Au-O-Ti interface is considered as the oxidation site. The crystallinity of the TiO_2 support have also an impact on the performance of the composites. The OER process was more efficient on Au/rutile than Au/anatase. This point was confirmed by Density Functional Theory (DFT). The result demonstrates that the calculated energy barrier, of the rate-determining step (the generation of *OOH intermediate), is smaller in the Au/rutile than that in Au/anatase interface (3.0 eV vs 3.6 eV, respectively).

Recent progress proved also a facet-dependent of the SC in POER over MNPs/SC photocatalytic system. The higher charge densities of some exposed facets of the semiconductors can significantly enhance the Stocky junction and therefore the spatial separation of the photoexcited electrons and holes (Bai et al., 2015). The oxidation state of the MNPs is also a decisive factor. In contract to the metallic Pt selectively active for PHER, its oxide form, particularly PtO, can promote either H_2 or O_2 evolution reactions and could efficiently decrease the kinetic overpotential and generate more active oxidation sites for water splitting (Fu et al., 2018; Li et al, 2017).

Other metal as Ir- and Ru-based materials are well known as one of the most effective photocatalyst for POER (Li et al., 2018). This is due to their specific local coordination environment facilitating water adsorption and oxygen evolution.

In general, the POER field is much less developed in comparison with the PHER field due to the challenge of this reaction which requires sophisticated and stable photocatalytic systems with appropriate oxidation capacity. Photoelectrochemical cell present a good alternative for performing one-pot photoassisted water splitting water splitting.

4.1.3. MNPs in photoassisted electrochemical water splitting

Electrochemical systems, using photovoltaic cell or integrated photoelectrodes, have been widely used for water splitting. In the Photoelectrochemical Cell (PEC), the working photoelectrode comprising supported plasmonic nanoparticles absorb photons and generate the electron-hole pairs. The holes generated in the working photoelectrode (anode) react with the H_2O to release oxygen (O_2) whereas, the photogenerated electrons are flowed through an external circuit to cathodic counter electrode and react with H^+ ions to evolve (H_2) (Fig 5). The stability of each electrode and/or MNPs/SC catalyst are strongly dependent on the pH of the electrolyte. However, the material corrosion, the limitations of transport as well as the OH absorption at the semiconductor surface present the main challenges in the photoassisted electrochemical water splitting system.

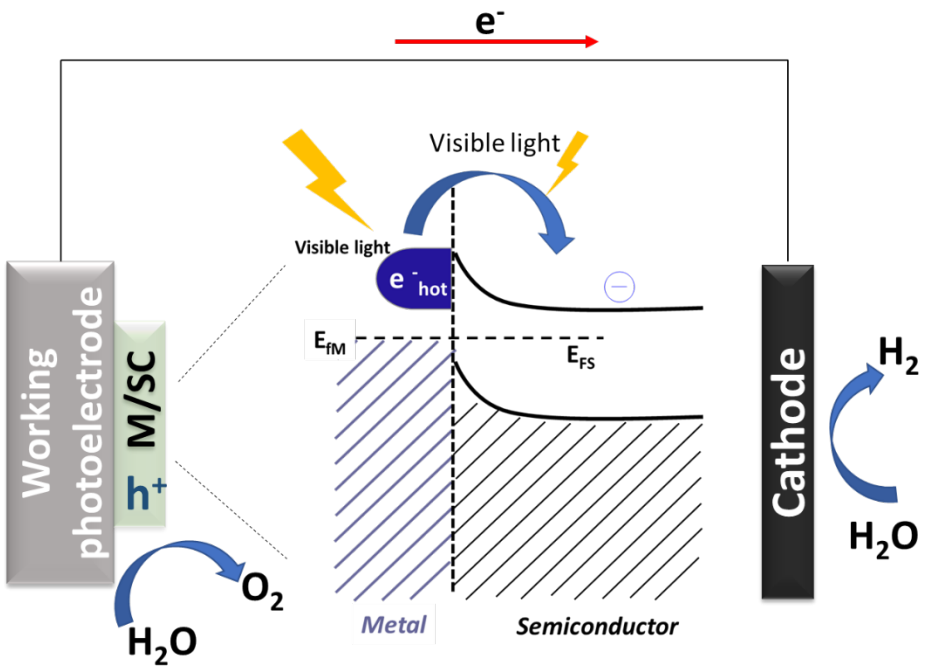

Fig. 5. General mechanism of photoassisted electrochemical water splitting in PEC.

4.2. MNPs in the photocatalytic reduction of CO_2

CO_2 is one of the most stable compounds among carbon compounds. CO_2 gas is linear and does not have a dipole moment. The one-electron reduction of CO_2 occurs at very negative potentials (-1.9 V vs ENH), due in part to the energy required for a structural rearrangement of the linear CO_2 to bridged $CO_2^{-\bullet}$. This energy is much higher than the potential for reducing the conduction bands of the available photocatalysts. Therefore, the reduction of CO_2 involves "activation", by adsorption to the active site of the photocatalyst, as a first step. This step is followed by the transfer of protons and multi-electrons to adsorbed/activated CO_2. It is produced at relatively low energies (-0.3 / -0.6V (NHE)). Depending on the routes and reaction conditions, different end products can be obtained. Thereafter, controlling the selectivity toward the desired

product (e.g., methanol, CO, etc.) is highly required in order to eliminate an additional separation process which can be expensive. On the other hand, the multi-electrons transfer process required for CO_2 reduction involves another important challenge in designing an efficient photocatalytic system by minimizing the recombination phenomenon. The induction of electrons from the photocatalyst conduction band to the adsorbed/activated CO_2 must occur more quickly than electron-hole recombination. However, the timescale of electron-hole recombination is generally 2-3 times faster than other electron transfer processes.

Plasmonic metals are extensively used for CO_2 photoreduction to maximize the lifetime of photogenerated charges, to activate the C=O bond of CO_2 and to generate the intermediate species. As for PHER, Pt-supported TiO_2 (Pt/TiO_2) was the most extensively employed system for selective formation of methane in CO_2 photoreduction (Wang et al., 2012; Xie et al., 2013; Xiong et al., 2017). This is due to its highest work function (5.65 eV) and better electron transfer ability to TiO_2 that is required for efficient CO_2 reduction. Pt is able to capture and accumulate the photogenerated electrons under UV irradiation form the SC valence band, facilitating then the CH_4 formation by 8-electrons transfer. DFT calculations and in-situ Fourier transform infrared spectroscopy (FTIR) measurements revealed that CO is an unmissable intermediate in the photocatalytic CO_2 reduction to CH_4 on Pt NPs according to the following pathway:

$CO_2 \rightarrow CO_2^- \rightarrow H_2CO_3 \rightarrow HCOOH \rightarrow CO \rightarrow HCHO \rightarrow CH_3OH \rightarrow CH_4$. (6)

The activity and selectivity of CO_2 photoreduction vs H_2 is highly dependent by the size of Pt NPs. By decreasing the size of Pt NPs the charge transfer efficiency increased, resulting in high performance of both CO_2 reduction and H_2 production, but with higher selectivity towards hydrogen over methane. It was demonstrated that the terrace sites of Pt nanoparticles favored CH_4 formation, however, the low blended sites are more active to generate the competitor hydrogen

((A) Dong et al., 2018). The photocatalytic CO_2 reduction can be significantly improved by constructing co-catalysts with high-indexed facet. PtCu alloy concave nanocubes with (730) facet deposited on C_3N_4 nanosheets, was found to be more efficient for selective production of CH_4 comparatively to PtCu (100) facet ((A) Lang et al., 2017). It was demonstrated that the adsorption and activation of CO_2 can be increased on the (730) high-index facets that contain more low-coordinated metal active sites. Comparing to Ag@Cu_2O, the Pt@Cu_2O showed a higher selectivity in the CO_2 conversion to CH_4 vs PHER (Wang et al., 2020).

AuNPs showed also good catalytic activity in the photoreduction of CO_2 into CH_4 under visible light. It can further react with the CO_2 to form CH_4 through a general mechanism illustrated in Fig. 6. Under visible light irradiation, the plasmonic MNPs (e.g. Au) transfer the hot electron to the SC conduction band. First, the H_2O is oxidized on MNPs hole to produce required H^+ for methane formation. The methane evolution takes place on the SC conduction band by the reduction of CO_2 in presence of H^+.

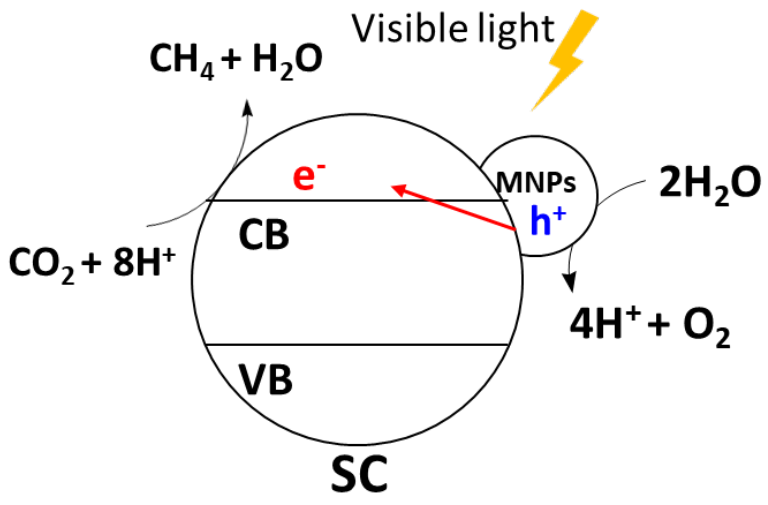

Fig. 6. General mechanism of CO_2 conversion to methane on MNPs/SC under visible light.

The incorporation of RuO_2 as co-catalyst with Au NPs enhances the CO_2 reduction selectivity toward CH_4, where Au NPs and RuO_2 NPs act as electron trapping agents and hole collectors, at the external surface, and the inner surface, respectively ((B) Dong et al., 2018). Ag based photocatalyst exhibited also a good CO_2 reduction. Ag NPs enhance the accumulation of the photogenerated electrons, required to achieve the multi-electron transfer's reaction (Xu et al., 2019). Introducing Ag NPs and intrinsic defects to TiO_2 can change the band gap of the photocatalyst which may enlarge the absorption of the samples in the visible light and the near-infrared regions and therefore enhance CO_2 photoreduction to obtain CO (Zhang et al., 2018). The effectiveness of CO_2 photoreduction over Ag-TiO_2 (anatase) samples, depends on the oxidation state of Ag (Handoko et al., 2019). For a material containing a mixture of Ag^0 and Ag^I, electron conduction and electron pool may occur on Ag^0, whereas adsorption of CO_2 or stabilization of some relevant intermediates may proceed on Ag^I.

The deposition of Pd on TiO_2 can enhance the selectivity of photoconversion of CO_2 to CO (Su, 2019). The twin defects on the surface of Pd nano-icosahedrons co-catalyst provide highly catalytic active sites for the activation of CO_2 molecules, and boosted the photocatalytic performance in CO_2 reduction to CO ((B) Lang et al., 2017). A comparison was reported concerning the effect of supporting different metals Pd and Au on the surface of layered $H_2SrTa_2O_7$ (HST) for CO_2 photoreduction (Chen et al., 2019). the Pd/HST sample displays the highest activity in the photocatalytic conversion of CO_2 to CO. However, Au/HST exhibits the highest activity in H_2 generation due to its relatively low overpotential for H_2. By taking into account the result with methane formation on Au/TiO_2 cited above, we conclude that the support also may play a crucial role on the reaction selectivity.

Mutli-carbon products were also produced from the photocatalytic reduction of CO_2 over some supported MNPs. Au@TiO_2 yolk–shell hollow spheres promote the formation of high-rank carbon species (C_2H_6), rarely obtained in the common CO_2 photocatalytic reductions. The formation of •CH_3 radical is the key step in this reaction. Here, Au NPs play an admitted role by generating a strong electric filed promoting the accumulation of the •CH_3 radicals with a high concentration on the TiO_2 surface. Then, a dimerization process is promoted and a C–C bond is formed (•CH_3 + •CH_3 → C_2H_6). Furthermore, for the TiO_2 relatively distant from the Au electromagnetic local field, a deficient amount of •CH_3 radicals may induce the formation of CH_4 through a combination with H^+ and e^-. CH_3OH and CO has been also produced during the photoreduction of CO_2 over Au NPs incorporated TiO_2 nanowires under low-energy visible light and Au loaded TiO_2 nanorods (brookite) under UV (365 nm) (Ohno et al., 2014; Tahir et al., 2015). Moreover, the production of formaldehyde was reported during the reduction of CO_2 over Au modified titanate species supported on SBA-15 under high-energy UV irradiation (Mei et al., 2013). The different facets of Pd photocatalyst found to have a strong effect on CO_2 photoreduction (Cao et al., 2012). The tetrahedral Pd nanocrystals with exposed {111} facets were more efficient to convert CO_2 compared to cubic Pd nanocrystals with exposed {100} facets. This was related to the different properties of the two facets regarding the charge transfer ability, the CO_2 adsorption energy and the desorption energy of CH_3-OH molecules.

Hybrid materials decorated with MNPs are also investigated in the photocatalytic reduction of CO_2. Au anchored in metal organic framework (MOF) structure (hybrids of thin porphyrin paddle-wheel framework-3 nanosheets PPF-3) exhibited high photocatalytic activity for CO_2 conversion into HCOOH in acetonitrile/ethanol solution under visible light. This material with nanosheet morphology can facilitate the accessibility of catalytic sites and accelerate the mass

and/or electron transfers. The efficiency of Au/MOF in the photoreduction of CO_2 into HCOOH was mainly related to plasmon resonance energy transfer. In this reaction, ethanol is playing the role of a hole scavenger and a proton source. A mixture of methanol/acetaldehyde is observed on Cu decorated graphene oxide (Cu/GO) (Shown et al., 2014). However, it is difficult to understand the role of copper in the CO_2 photoreduction due to the co-existence of different valence/forms and the possible interchange between them during the reaction. The co-existence of Cu(I) and Cu(0) was beneficial for the CO_2 photoreduction, while an excess of Cu(0) was undesirable for the reaction. It was also reported that Pd-based photocatalyst not only favor the photoreduction of CO_2 to CO and CH_4, but also could enhance the selectivity towards other products like: HCOOH (Raja et al., 2011) and C_2H_6 (Hong et al., 2014).

Metal clusters displayed also some efficiency in the CO_2 photoreduction. Single silver atoms, confined into the layered channels of hollandite manganese dioxides (HMO) as semiconductor support, show high efficiency to convert CO_2 to CH_4 under visible irradiation which was 1.52 folds higher that of silver nanoparticles. This revealed that downsizing noble metal to single atomic level on the surface of photocatalysts may maximize the fraction of accessible active sites for the adsorption and the activation of CO_2 (Ding et al., 2019). The stabilized silver clusters by polymethacrylic acid (AgNCs-PMAA) on TiO_2 nanoparticles exhibit a remarkable efficiency for the reduction of CO_2 to CO under visible light (Zhang et al., 2018). This is due to the electron transfer from the CB of TiO_2 to the LUMO (~0.26 eV) of Ag clusters (Cheng et al., 2012). Similarly, the presence of Pt octamer clusters on the surface of TiO_2 (101) (Yan et al.., 2018) promotes the first step of the CO_2 reduction by strong adsorption of $HCOO^-$ and OH^- species. The enhanced CO_2 adsorption strength at Pt clusters is mainly related to the formation of strong bonding orbitals between the molecular states of CO_2 with d-orbital of Pt which increase the charge

accumulation in CO_2 surface and facilitate the formation of the CO_2^- anion intermediate. The formation of this anion is the first and decisive step for the reduction process (Yang et al., 2014).

Despite the advance in the use of the MNPs in the CO_2 reduction the main challenge resides in the competitive reduction reaction of protons vs CO_2 on the MNPs.

4.3. MNPs in green chemistry

4.3.1. MNPs in the Selective photooxidation of alcohol

The alcohols oxidation to carbonylic derivatives is a great practical interest in the synthesis of valuable chemical intermediates (Mallat et al., 2004; Enache et al., 2004). However, the conventional oxidation methods for alcohols using highly harsh oxidants (i.e., chromates and permanganates) can produce environmentally harmful waste (Metzger et al., 1998; Menger et al., 1981). Therefore, the introduction of catalytic systems using molecular oxygen from air is preferred for a greener and cheaper process. MNPs is often used in the selective photooxidation process. The application of gold nanoparticles dispersed on carbonic supports where reported early for thermal oxidation of ethylene glycol, D-glucose, glycerol and phenylethane-1,2-diol under O_2 (Prati et al., 1999). However, a high temperature and O_2 pressure were required causing a selectivity issue. Basing on the knowledge of SPR beneficial effect of metallic nanoparticles in photocatalysis, well detailed above, its application was extended to alcohol selective photooxidation under milder conditions. The Numerous models of Au/TiO_2 systems reported in the literature aim to obtain a better selectivity and enhanced activity. The oxidation of alcohol takes place on electron-deficient MNPs surface to compensate the charge after the electron transfer from the MNPs to the excited semiconductor. In case of TiO_2, the molecular O_2 is first reduced on TiO_2 surface to generate O_2^- which interact with alcohol's hydrogen to produce H_2O or H_2O_2 as

by-product with the desired aldehyde or ketone. (**Fig. 7 top**). In the photooxidative process a high yield can be obtained under mild condition (room temperature, low pressure) which avoid the selectivity issues. However, a direct oxidation of the alcohol and/or subproducts on TiO_2 cannot be excluded. Thus, minimizing this undesired reaction can enhance the selectivity toward partial oxidation vs total oxidation.

Different Au/TiO_2 photocatalysts were tested in the selective oxidation of alcohol. The variety of these systems comes from the structural and shape of TiO_2 and/or AuNPs designed from various synthetic procedure. Three distinguish roles of AuNPs in the selective alcohol oxidation, have been reported in the literature. This totally depends on the environment of the NPs. E.g. Tsukamoto et al. (2012) demonstrate that the heterojunction of TiO_2 composed from anatase and rutile promote the migration of AuNPs and their stabilization at the anatase/rutile interface (**Fig. 7 a**). The activity was increased by 5 times in comparison with that of AuNPs supported on pure anatase TiO_2 and tested under similar condition. The photocatalytic improvement of TiO_2 containing heterojunction site was explained by the following process: The thermodynamically favored electron accumulation in the conduction band (CB) of rutile can realign the energy level which allows the electron transfer from rutile to anatase (**Fig. 7 a**). This charge separation at the interface enables smooth e^- transfer from the photoactivated Au particles to TiO_2 and consequently a more efficient photocatalytic activity.

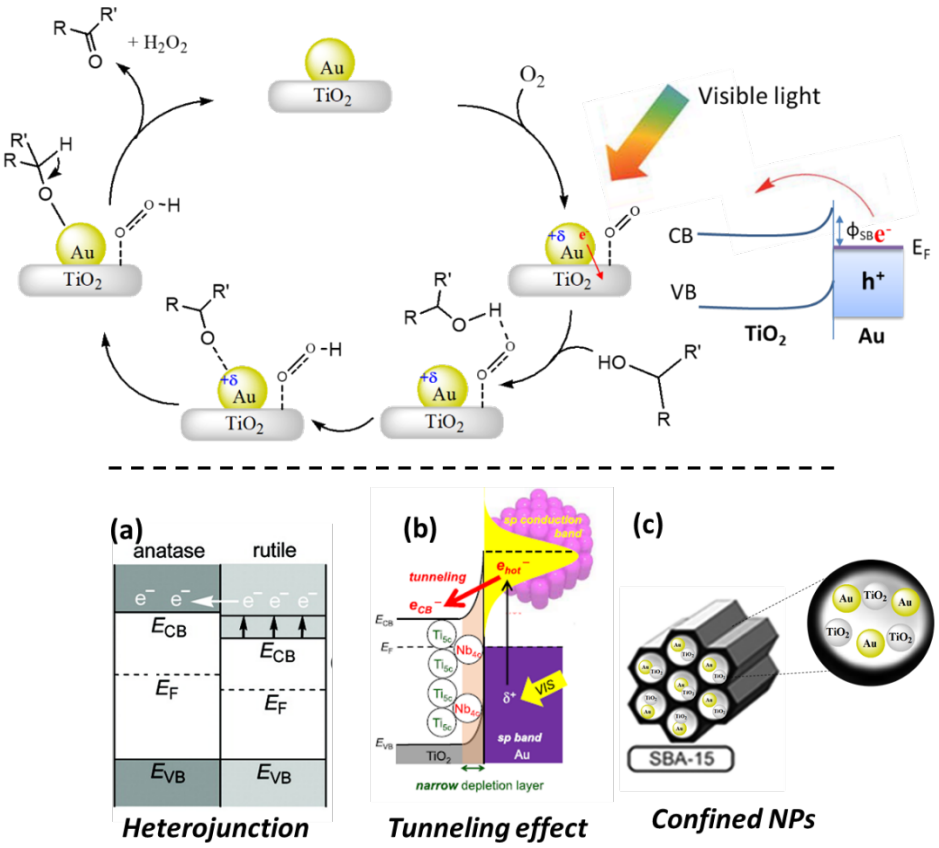

Fig. 7. Top: General mechanism of isopropanol photooxidation with AuNPs@TiO_2, Bottom: different configuration of Au/TiO_2 systems used in selective oxidation of alcohol. Copyright 2012 and 2019 American Chemical Society. Reprinted with permission from Tsukamoto el al. 2012 and Shiraishi et al. 2019.

However, one of the major challenges in Au/TiO_2 photocatalytic system is the ability of a hot electron to overcome the Schottky barrier between AuNPs and TiO_2. Introducing Lewis acid species (e.g. Nb^{5+}) in the system can limit this phenomenon (**Fig. 7b**) (Shiraishi et al., 2019). The cations neutralize the negative charge of the Au particles and results in a narrower depletion of the Schottky barrier. However, loading an excess amount of Nb^{5+} lead to the formation of polynuclear Nb_2O_5 aggregates which decrease the electron density of Au particles as well as their SPR absorption.

The increase of the interfacial area between Au and TiO_2 can be achieved by the elaboration of Au and TiO_2 particles with comparable size. In this context, the synthesis of nanosized Au and TiO_2 seems like a convenient approach but still suffer from NPs agglomeration. This issue was avoided by the preparation of AuNPs (4 nm) and TiO_2NPs (6.4 nm) in the SBA-15 channels to obtain the Au/TiO_2 composite uniformly dispersed in the channels of SBA-15 (Au/TiO_2/SBA-15) (**Fig. 7c**) (Chen et al., 2015). The plasmonic composite was applied in photooxidation of benzyl alcohol and its activity was compared with conventional AuNPs supported on anatase/rutile TiO_2 composite (Au@P25). Interestingly, the composite Au/TiO_2/SBA-15 was two times more efficient than Au@P25. Additionally, the recombination of charge carriers could be largely decreased due to the large interfacial area between Au and the small TiO_2 particles. On the other hand, the SBA-15 presents a high affinity to alcohol which decrease the diffusion limit of substrate.

Compared to AuNPs, few works where reported using other MNPs. For example, RuNPs (<5 nm) dispersed on TiO_2 nanobelt was tested on photooxidation of benzyl alcohol in gas phase at 250 °C. Contrariwise to plasmonic NPs, the UV irradiation was required to obtain benzaldehyde with 80 % of yield (Tian et al., 2016). RuNPs was also supported on magnetic N doped carbon (Ru@N-C) in order to be recycled by applying an external magnetic field to isolate the supported catalyst (Dabiri et al., 2019). In contrast to TiO_2, Ru@N-C showed an absorption band at 420 nm which render it active under visible light irradiation to yield 90 % of benzaldehyde.

The application of the MNPs for the selective oxidation under mild conditions open the routes for other applications in catalysis, where the hydrothermal factors promotes the overoxidation of the desired product.

4.3.2. MNPs in formic acid reforming and photoassisted SCR

In a very recent study performed by our group, sub-nanometer silver clusters trapped into faujasite framework (Ag@ZX-V) shows an interesting activity in the formic acid reforming (El-Roz et al., 2018) and photoassisted Selective Catalytic Reduction (SCR) with NH_3 (Hamoud et al., 2019) at RT and under visible light. In liquid phase, it was shown that the generated sub-nanosized Ag clusters excited by visible light exhibit a strong stability (16 h of reaction), good activity and high selectivity (> 99%) for the decomposition of formic acid into H_2 and CO_2. (**Fig 8 a**) This reaction is proposed as a reversible chemical storage of H_2 and suffer from the low selectivity to form CO when a semiconductor is used. This high performance of the Ag@ZX-V was attributed to the LSPR effect of silver nanoclusters and the formation of the AgNPs during the reaction (Fig. 5a). The same sample demonstrates an efficiency in the deNO_x via photoassisted SCR reaction at a relatively low temperature (150°C) in gas phase. At RT, the silver clusters induce selective photo-oxidation reactions of NH_3 due to the formation of highly oxidant singlet oxygen via an energy transfer from the excited silver clusters/NPs to the triplet of oxygen: $NH_3 \xrightarrow{^1O_2} \bullet NH_2 \xrightarrow{^1O_2} NO$ (Fig. 5b). However, increasing the temperature to 150°C promotes the SCR process vs the oxidation and a conversion of 18% of NO_x to N_2 was occurred. This was attributed to the plasmonic local heating of silver clusters which can promote intermediate species e.g. NH_2NO and NH_2NO_2 inducing the reduction of NO_x (**Fig. 8 b**).

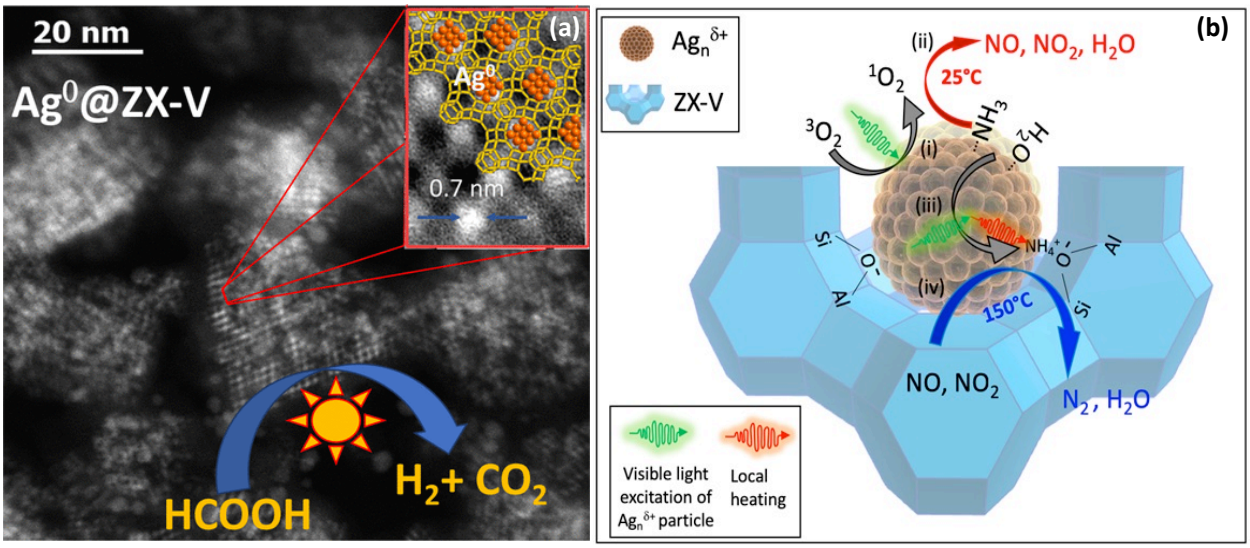

Fig. 8. a) The decomposition of formic acid into H_2 and CO_2 over Ag^0@ZX-V under visible light (liquid phase) and b) the proposed photo-SCR reaction mechanisms at RT and T=150 °C over Ag@ZX-V catalyst (El-Roz **et al.**, 2018; Hamoud **et al.**, 2019). Copyright 2018 and 2019 American Chemical Society and Elsevier, respectively. Reprinted with permission from El-Roz et al. 2018 and Hamoud et al. 2019.

4.3.3. MNPs for Nitroaromatic photoreduction

The nitroaromatic reduction is an important method to produce anilines or azo compounds which are very useful in pharmaceutical, pesticides, dyes and other synthesis (Kahl et al., 2000; Ali et al., 2018).

Earlier, the photo-assisted selective reduction of nitroaromatics toward anilines was applied by using the TiO_2 (P25) under UV irradiation (Bresova et al., 1997). In order to achieve a better charge separation, AgNPs (1.5 nm) was introduced to TiO_2 by photodeposition method. The reduction of nitrobenzene was tested under UV irradiation in methanol to obtain selectively the aniline with a two times faster reaction rate than that with P25. However, the application under visible light irradiation still much more attractive. In this context, AuNPs was photo-deposited on Ag-TiO_2 to

obtain Ag-TiO_2/AuNPs composite with absorption band around 550 nm (Tanaka et al., 2013). The catalysts were used for nitrobenzene reduction under visible light in isopropanol to obtain selectively the aniline with acetone as oxidation product of isopropanol.

ZrO_2 was applied as inert support for AuNPs and the material was directly used for nitroaromatic reduction under visible light. Interestingly the selectivity was exclusively oriented toward the azo compounds. On the other hand, the alloys Au-Cu@ZrO_2 prepared in the same conditions produces only aniline products. Herein the bond strength between the reaction components with metal can be crucial for the reaction selectivity (Zhu et al., 2010; Xiao et al., 2016). The reaction orientation toward aniline or azo compound was also possible with AuNPs@Al_2O_3 by using two different sources of hydrogen. By using HCOOH no coupling (azo) product was obtained and the reaction was completely oriented towards the formation of aniline (Chaiseeda et al., 2017). The role of the AuNPs is to generate hot electrons and holes at surfaces which further generate AuNPs−H species by abstracting hydride from a hydrogen donor (e.g. isopropanol) and leaving acetone as oxidized product. This Au−H bond is relatively stable at the AuNPs surface which transfers hydride to nitroarene and regenerate the catalyst. Furthermore, two hydrides transfer leads to the formation of nitroso-arene by eliminating water. Then nitroso-arene hydrogenation leads to the hydroxylamine which is the key intermediate in this catalytic process. The hydroxylamine is then converted to aniline (pathway A, **Fig. 9**) or to the azoarene after the hydroxylamine coupling with nitroso-arene (pathway B, **Fig. 9**).

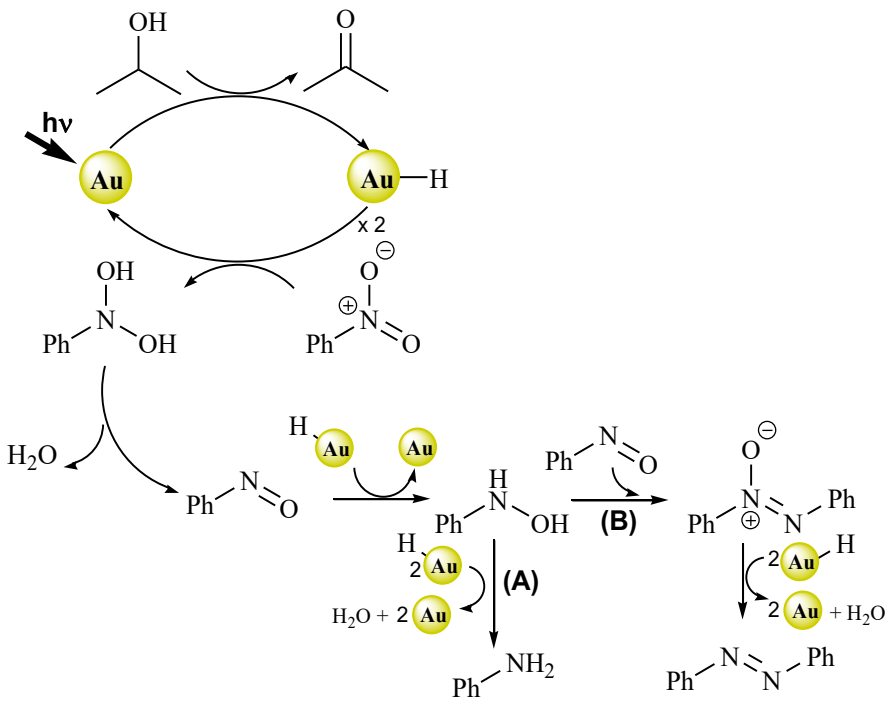

Fig. 9. Detailed mechanism for the direct photoreduction of nitroarene on gold nanoparticle.

Metal oxides with oxygen vacancies H_xMoO_{3-y} have attract much attention as a plasmonic alternative to conventional noble metals which also acts as metallic nanoparticles support (Cheng et al., 2016). These materials were applied as support for PdNPs, RuNPs and both of Pd and RNPs in paranitrophenol (PNP) reduction using H_2 for depollution purposes/ The mechanism consists in the adsorption of PNP over nitro group and H_2 (formation of hydride) over Pd surface. The excited electrons of plasmonic H_xMoO_{3-y} supports are quickly transferred to the surface of the metal NPs under visible light to assist the hydrogenation of nitro groups resulting in the formation of the paraaminophenol (PAP).

4.3.4. MNPs for Photoassisted carbon-carbon cross coupling

C−C coupling reactions is one of the most important strategies in synthetic organic chemistry. Palladium-catalyzed cross-coupling methodologies have revolutionized synthetic organic chemistry and honored by Nobel prize in 2010 *"for palladium-catalyzed cross couplings in organic synthesis"* (Echavarren et al., 2010). The aptitude to break the aryl-halogen bond is a determinant factor in the cross-coupling reactions. This process consists offering an electron donation from M (e.g. Pd) to the antibonding orbital LUMO of substrate which weaken the aryl-halogen bond. Consequently, a large number of organometallic complexes with different electronic properties were reported in this field (Buchwald, 2008). Depending of the substrate, the reaction is oriented toward:

- *Suzuki-Miyaura* when aryl boronic acid is incorporated to obtain aryl-aryl bond.
- *Heck-Mizoroki* when vinyl group is employed to prepare polysubstituted alkenes
- *Sonogashira coupling* when a terminal alkyne is used to obtain disubstituted alkynes.

Photo-assisted electrons transfers from MNPs surface to the LUMO of the substrate is a famous strategy to achieve a better activity. Several studies on PdNPs (supported on semiconductive supports or alloyed with gold) were reported for developing light driven Suzuki-Miyaura, Sonogashira and Heck-Mizoroki coupling. The overall mechanistic pathway of these photocatalytic systems consists in the generation of an electron-hole pairs by the excitation of the semiconductor upon light irradiation (UV or/and visible). This is followed by the transfer of the photoexcited electrons to Pd. Electron-rich Pd^0 then undergoes oxidative addition of aryl-halogen. The first reported system for Suzuki cross coupling was proposed in 2013 where Pd NPs was deposited on mesoporous carbon nitride (g-C_3N_4) (Li et al., 2013). The composite was used to catalyze the Suzuki-Miyaura coupling of iodobenzene and benzeneboronic acid under UV-visible

light irradiation at room temperature. However, the product yield was decreased by filtering off the UV part of the Xenon lamp. An activity improvement under visible light was then reported by doping the Pd@g-C_3N_4 with reduced graphene oxide (rGO) (Zhao et al., 2019). The electron transfer from the semiconductor to Pd is directly related the band gap value of the semiconductor (2.7 eV for g-C_3N_4). Thus, the choice of a support with a lower band gap that absorb visible light may explain the higher photocatalytic efficiency. In this context, Silicon Carbide (SC) with low band gap (~2.4 eV) was proposed as a support of PdNPs (Jiao et al., 2015). Among all, Pd@SiC was the much efficient for Suzuki-Miyaura of iodobenzene and phenylboronic acid coupling under visible light at 30°C where the recorded TOF is 1053 h^{-1} versus 304 h^{-1} and 523 h^{-1} for g-C_3N_4, rGO-doped g-C_3N_4, respectively. Conjugated porous polymers, combining semiconductive π-conjugated skeletons with permanent pores have been also used as supports for Pd NPs for photo-assisted Suzuki-Miyaura coupling. For example, the PdNPs supported on the conjugated microporous poly(benzoxadiazole) network (B-BO_3) (Wang et al., 2015), were efficient for the aryl-bromide or aryl iodide coupling with phenyl boronic acid. Additionally, it was reported that the Conjugated Nanoporous Polycarbazole (CNP) with the lower band gap (2.0 eV) is highly active for photocatalytic activation of aryl chlorides in the Suzuki-Miyaura coupling i(Guo et al., 2019). This is a very challenging topic due to the inert nature of the C-Cl bond which generally needs excess strong base and high temperature to be activated (Barder et al., 2005).

Other works proposed the use of gold nanoparticles to enriches the Pd NPs by hot electron coming from SPR upon exciting AuNPs under Vis-NIR irradiation (Wang et al., 2013). (Xiao et al., 2014). A significant enhancement of the activity of Au-Pd alloy systems was reported.

For Sonogashira coupling a deprotonation of terminal alkyne is required to be coordinated with Pd metal. Pd@SiC used in Suzuki-Miyaura coupling was also reported for Sonogashira coupling

by introducing phenylacetylene instead of boronic acids (Wang et al., 2017). A good activity was observed in the activation of the aryl-bromide and aryl-iodide. However, a relatively high temperature (120 °C) was required. TiO_2 (P25) was also reported as a support for Pd NPs for Sonogashira coupling (Elhage et al., 2018). Contrary to Pd@SiC, this catalyst was very efficient at room temperature under 425-nm LED irradiation.

The application of MNPs in the photo-assisted C-C coupling was successfully extended to Heck-Mizoroki coupling which is a powerful tool for the preparation of polysubstituted alkenes (Heck et al., 2004). In this process, the coupling product is obtained from a fast coordination–insertion process of alkenes to the Ar–Pd–I complex followed by β-hydrogen elimination. PdNPs supported on CNC was reported in Heck-Mizoroki coupling, showing a good overall performance under visible light (Guo et al. 2016). On the other hand, a more sophisticated magnetic support constituted from rGO, Multi-Walled-Carbon-Nanotubes (MWCNT) and $CaFe_2O_4$ (Pd-rGO/CNT/$CaFe_2O_4$) was also used as a support for PdNPs showing a good activity with iodoaryle and a remarkable recyclability by applying an external magnetic field to isolate insoluble catalytic materials (Bagherzadeh el al. 2019).

The different pathways demonstrating the active involvement of the MNPs in the photoassisted green chemistry, are illustrated in **Fig. 10.**

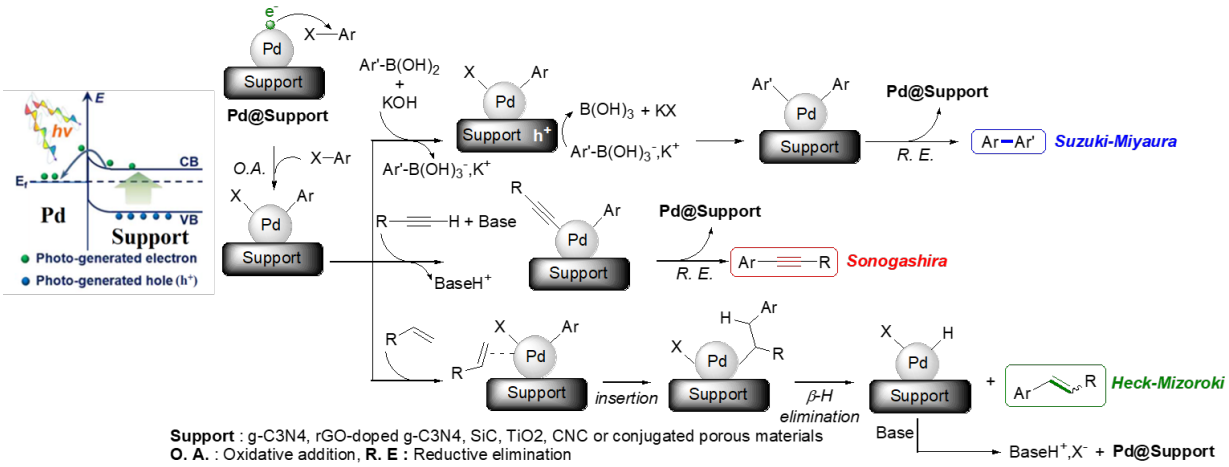

Fig. 10. Plausible mechanistic pathways for photo-assisted Suzuki-Miyaura, Sonogashira and Heck-Mizoroki coupling using Pd@Support as photocatalyst model.

5. Conclusion

This chapter describes the development of metal nanoparticles in photocatalysis by presenting the fundamental theoretical aspects as well as the research progresses in this field according to three applications: 1. Photocatalytic water splitting; 2. Photocatalytic CO_2 reduction; 3. and photoassited Green chemistry. The characteristic driving forces of the photocatalytic activity of MNPs/support are related to the LSPR of the MNPs, the enhanced charge carrier separation as well as the local heating. Furthermore, the catalytic activity can be related to other intrinsic properties such as: the MNPs size, the MNPs/Photocatalyst interface area and the nature of the supports (inert or semiconductor). Extrinsic factors can also impact the activity of the MNPs photocatalyst based system. Depending of the reaction condition the MNPS can act with the reactants as electron donor (reduction) or electron acceptor (oxidation). This depends on different factors as the reactant nature, the reaction conditions (temperature, pressure, atmosphere), the support as well as the irradiation wavelength. In another word, depending of the intrinsic and extrinsic factors, the same MNPs provides the active sites for water oxidation to produce O_2 or for protons reduction to

produce H_2. In the case of CO_2 reduction or green chemistry, the selectivity can be oriented according to the choice of the MNPs.

Despite the interest offered by the use of the MNPs in photocatalysis for converting light energy into chemical energy, this technology seems to be a bit far from commercialization. The main issue before reaching this objective is mainly related to the lack in stability of the MNPs under irradiation leading to changes in the material morphology and consequently loss of catalytic performance. In addition, in most of the applications, artificial UV light sources are required. However, many recent research efforts demonstrated that the choice of the support can significantly enhance the stability of the MNPs and/or their performance under solar light.

6. Acknowledgment

Authors acknowledge the PHC Tassili and the "RIN recherche 2018" programe (Normandie region) for the financial support via and the projects "17MDU983" and "RAPHYD", respectively.

7. References

Abe, R.; Sayama, K.; Arakawa, H. Significant effect of iodide addition on water splitting into H_2 and O_2 over Pt-loaded TiO_2 photocatalyst: suppression of backward reaction. Chem. Phys. Lett. 2003, 371, 360-364.

Ali, Y.; Hamid, S. A.; Rashid, U. Biomedical applications of aromatic azo compounds. *Mini Rev. Med. Chem.* **2018,** *18*, 1548-1558.

Arinze, E. S.; Qiu, B.; Nyirjesy, G.; Thon, S. M. Plasmonic nanoparticle enhancement of solution-processed solar cells: practical limits and opportunities. *ACS Photonics.* **2016**, *3*, 158-173.

Attia, Y.; Samer, M. Metal clusters: New era of hydrogen production. *Renew. Sust. Energ. Rev.* **2017**, *79*, 878-892.

Bagherzadeh, M.; Kaveh, R.; Mahmoudi, H. Facile synthesis of a recyclable Pd-rGO/CNT/$CaFe_2O_4$ nanocomposite with high multifunctional photocatalytic activity under visible light irradiation. *J. Mater. Chem. A* **2019** *7*, 16257-16266.

Bai, S.; Li, X.; Kong, Q.; Long, R.; Wang, C.; Jiang, J.; Xiong, Y. Toward enhanced photocatalytic oxygen evolution: synergetic utilization of plasmonic effect and Schottky junction via interfacing facet selection. *Adv. Mater*. **2015**, *27*, 3444-3452.

Barder; T. E.; Walker, S. D.; Martinelli, J. R.; Buchwald, S. L. Catalysts for Suzuki− Miyaura coupling processes: scope and studies of the effect of ligand structure. *J. Am Chem. Soc.* **2005**, *127*, 4685-4696.

Beasley, C.; Kumaran Gnanamani, M.; Santillan-Jimenez, E.; Martinelli, M.; Shafer, W. D.; Hopps, S. D.; Kim, D. Y. Effect of Metal Work Function on Hydrogen Production from Photocatalytic Water Splitting with $MTiO_2$ Catalysts. *ChemistrySelect.* **2020**, *5*, 1013-1019.

Belloni, J. Nucleation, growth and properties of nanoclusters studied by radiation chemistry: application to catalysis. *Catal. Today*. **2006**, *113*, 141-156.

Berto, T. F.; Sanwald, K. E.; Byers, J. P.; Browning, N. D.; Gutiérrez, O. Y.; Lercher, J. A. Enabling overall water splitting on photocatalysts by CO-covered noble metal co-catalysts. *J. Phys. Chem. Lett.* **2016**, *7*, 4358-4362.

Brezova, V.; Blažková, A.; Šurina, I.; Havlinova, B. Solvent effect on the photocatalytic reduction of 4-nitrophenol in titanium dioxide suspensions. *J. Photochem. Photobiol. A.* **1997**, *107*, 233-237.

Buchwald, S. L. Cross coupling. *Acc. Chem. Res*. **2008**, *41*, 1439.

Cao, S.; Li, Y.; Zhu, B.; Jaroniec, M.; Yu, J. Facet effect of Pd cocatalyst on photocatalytic CO_2 reduction over g-C_3N_4. *J. Catal.* **2017** *349*, 208-217.

Chaiseeda, K.; Nishimura, S.; Ebitani, K. Gold nanoparticles supported on alumina as a catalyst for surface plasmon-enhanced selective reductions of nitrobenzene. *ACS Omega* **2017**, *2*, 7066-7070.

Chen, H.; Wang, Q.; Lyu, M.; Zhang, Z. Wang, L. Wavelength-switchable photocurrent in a hybrid TiO_2–Ag nanocluster photoelectrode. *ChemComm*. **2015**, *51*, 12072-12075

Chen, W.; Wang, Y.; Shangguan, W. Metal (oxide) modified (M= Pd, Ag, Au and Cu) $H_2SrTa_2O_7$ for photocatalytic CO_2 reduction with H_2O: The effect of cocatalysts on promoting activity toward CO and H_2 evolution. *Int. J. Hydrogen. Energ.* **2019**, *44*, 4123-4132.

Chen, Y.; Li, W.; Wang, J.; Yang, Q.; Hou, Q.; Ju, M. Gold nanoparticle-modified TiO_2/SBA-15 nanocomposites as active plasmonic photocatalysts for the selective oxidation of aromatic alcohols. *RSC Adv.* **2015**, *6*, 70352-70363.

Cheng, H.; Wen, M.; Ma, X.; Kuwahara, Y.; Mori, K.; Dai, Y.; ... Yamashita, H. Hydrogen doped metal oxide semiconductors with exceptional and tunable localized surface plasmon resonances. *J. Am. Chem. Soc.* **2016**, *138*, 9316-9324.

Cheng, J.; Gao, C.; Jing, M.; Lu, J.; Lin, H.; Han, Z. Zhang, D. Photo-catalysis water splitting by platinum-loaded zeolite A. *Mater. Res. Express* **2018**, *5*, 055506.

Chouhan, N. *Silver nanoparticles: synthesis, characterization and applications;* BoD – Books on Demand, 2018; pp 21-56.

Comin, A.; Manna, L. New materials for tunable plasmonic colloidal nanocrystals. *Chem. Soc. Rev.* **2014**, *43*, 3957-3975.

Dabiri, M.; Nikbakht, R.; Movahed, S. K. Structuring Ru nanoparticles on magnetic nitrogen doped carbon induces excellent photocatalytic activity for oxidation of alcohols under visible light. *J. Photochem. Photobiol. A*. **2019**, *379*, 159-170.

Davies, P. W. Organometallics: transition metals in organic synthesis. *Annu. Rep. Prog. Chem. Sect. B: Org. Chem.* **2009**, *105*, 93-112.

Ding, J.; Liu, X.; Shi, M.; Li, T.; Xia, M.; Du, X. Zhong, Q. Single-atom silver–manganese catalysts for photocatalytic CO_2 reduction with H_2O to CH_4. *Sol. Energy Mater Sol*. **2019**, *195*, 34-42.

(A) Dong, C.; Lian, C.; Hu, S.; Deng, Z.; Gong, J.; Li, M.; ... Zhang, J. Size-dependent activity and selectivity of carbon dioxide photocatalytic reduction over platinum nanoparticles. *Nat. Commun.* **2018**, *9*, 1-11.

(B) Dong, C.; Hu, S.; Xing, M.; Zhang, J. Enhanced photocatalytic CO_2 reduction to CH_4 over separated dual co-catalysts Au and RuO_2. *Nanotechnology*. **2018**, *29*, 154005.

Echavarren, A. M. Nobel Prize Awarded for Catalysis. *ChemCatChem.* **2010**, *2*, 1331-1332.
Elhage, A.; Lanterna, A. E.; Scaiano, J. C. Light-induced Sonogashira C–C coupling under mild conditions using supported palladium nanoparticles. *ACS Sustain. Chem. Eng.* **2018**, *6*, 1717-1722.

El-Roz, M.; Telegeiev, I.; Mordvinova, N. E.; Lebedev, O. I.; Barrier, N.; Behilil, A. Valtchev, V. Uniform generation of sub-nanometer silver clusters in zeolite cages exhibiting high photocatalytic activity under visible light. *ACS Appl. Mater.* **2018***, 10*, 28702-28708.

Enache, D. I.; Edwards, J. K.; Landon, P.; Solsona-Espriu, B.; Carley, A. F.; Herzing, A. A. Hutchings, G. J. Solvent-free oxidation of primary alcohols to aldehydes using Au-Pd/TiO_2 catalysts. *Science*. **2006**, *311*, 362-365.

Fu, S.; Zhang, B.; Hu, H.; Zhang, Y.; Bi, Y. ZnO nanowire arrays decorated with PtO nanowires for efficient solar water splitting. *Catal. Sci. Technol.* **2018**, *8*, 2789-2793.

Fu, X.; Cai, J.; Zhang, X.; Li, W. D.; Ge, H.; Hu, Y.. Top-down fabrication of shape-controlled, monodisperse nanoparticles for biomedical applications. *Adv. Drug Deliv. Rev.* **2018**, 132, 169-187.

Fujishima, A.; Honda, K. Electrochemical photolysis of water at a semiconductor electrode. *Nature.* **1972**, *238*, 37-38.

Gomes Silva, C.; Juárez, R.; Marino, T.; Molinari, R.; García, H. Influence of excitation wavelength (UV or visible light) on the photocatalytic activity of titania containing gold nanoparticles for the generation of hydrogen or oxygen from water. *J. Am. Chem. Soc.* **2011**, *133*, 595-602.

Guo, X. W.; Hao, C. H.; Wang, C. Y.; Sarina, S.; Guo, X. N.; Guo, X. Y. Visible light-driven photocatalytic Heck reaction over carbon nanocoil supported Pd nanoparticles. *Catal. Sci. Technol*. **2016**, *6*, 7738-7743.

Guo, B.; Li, H. X.; Zha, C. H.; Young, D. J.; Li, H. Y.; Lang, J. P. Visible-Light-Enhanced Suzuki–Miyaura Reactions of Aryl Chlorides in Water with Pd NPs Supported on a Conjugated Nanoporous Polycarbazole. *ChemSusChem*. **2019**, *12*, 1421-1427.

Hamoud, H. I.; Lafjah, M.; Douma, F.; Lebedev, O. I.; Djafri, F.; Valchev, V. El-Roz, M. Photo-assisted SCR over highly dispersed silver sub-nanoparticles in zeolite under visible light: An Operando FTIR study. *Solar Energy*. **2019**, *189*, 244-253.

Han, J.; Liu, Y.; Guo, R. Facile synthesis of highly stable gold nanoparticles and their unexpected excellent catalytic activity for Suzuki− Miyaura cross-coupling reaction in water. *J. Am. Chem. Soc*. **2009**, *131*, 2060-2061.

Han, P.; Martens, W.; Waclawik, E. R.; Sarina, S.; Zhu, H. Metal nanoparticle photocatalysts: synthesis, characterization, and application. *Part. Part. Syst. Charact.* **2018**, *35*, 1700489.

Handoko, C. T.; Moustakas, N. G.; Peppel, T.; Springer, A.; Oropeza, F. E.; Huda, A. Strunk, J. Characterization and effect of Ag (0) vs. Ag (I) species and their localized plasmon resonance on photochemically inactive TiO_2. *Catalysts*. **2019**, *9*, 323.

Hao, E.; Schatz, G. C. Electromagnetic fields around silver nanoparticles and dimers. *J. Chem. Phys.* **2004**, *120*, 357-366.

Heck, R. F. Palladium-catalyzed vinylation of organic halides. *Org. React*. **2004**. *27*, 345-390.

Hisatomi, T.; Takanabe, K.; Domen, K. Photocatalytic water-splitting reaction from catalytic and kinetic perspectives. *Catal. Lett.* **2015**, *145*, 95-108.

Hong, J.; Zhang, W.; Wang, Y.; Zhou, T.; Xu, R. Photocatalytic reduction of carbon dioxide over self-assembled carbon nitride and layered double hydroxide: the role of carbon dioxide enrichment. *ChemCatChem*. **2014**, *6*, 2315-2321.

Hu, H.; Qian, D.; Lin, P.; Ding, Z.; Cui, C. Oxygen vacancies mediated in-situ growth of noble-metal (Ag, Au, Pt) nanoparticles on 3D TiO_2 hierarchical spheres for efficient photocatalytic hydrogen evolution from water splitting. *Int. J. Hydrogen Energ.* **2020**, *45*, 629-639.

Huang, X.; El-Sayed, I. H.; Qian, W.; El-Sayed, M. A. Cancer cell imaging and photothermal therapy in the near-infrared region by using gold nanorods. *J. Am. Chem. Soc.* **2006**, *128*, 2115-2120.

Hunt, L. B. The true story of Purple of Cassius. *Gold Bull.* **1976**, *9*, 134-139.

Ilawe, N. V.; Oviedo, M. B.; Wong, B. M. Effect of quantum tunneling on the efficiency of excitation energy transfer in plasmonic nanoparticle chain waveguides. *J. Mat. Chem. C.* **2018**, *6*, 5857-5864.

Jaramillo, T. F.; Jørgensen, K. P.; Bonde, J.; Nielsen, J. H.; Horch, S.; Chorkendorff, I. Identification of active edge sites for electrochemical H_2 evolution from MoS_2 nanocatalysts. *Science*. **2007**, *317*, 100-102.

Jeong, S. Y.; Shin, H. M.; Jo, Y. R.; Kim, Y. J.; Kim, S.; Lee, W. J. An, H. Plasmonic silver nanoparticle-impregnated nanocomposite $BiVO_4$ photoanode for plasmon-enhanced photocatalytic water splitting. *J. Phys. Chem. C.* **2018**, *122*, 7088-7093.

Jiao, Z.; Zhai, Z.; Guo, X.; & Guo, X. Y. Visible-light-driven photocatalytic Suzuki–Miyaura coupling reaction on Mott–Schottky-type Pd/SiC catalyst. *J. Phys. Chem. C.* **2015**, *119*, 3238-3243.

Kale, M. J.; Avanesian, T.; Xin, H.; Yan, J.; Christopher, P. Controlling catalytic selectivity on metal nanoparticles by direct photoexcitation of adsorbate–metal bonds. *Nano lett*. **2014**, *14*, 5405-5412.

Kale, M. J.; Avanesian, T.; Christopher, P. Direct photocatalysis by plasmonic nanostructures. *Acs Catal.* **2014,** *4*, 116-128.

Kahl, T.; Schröder, K. W.; Lawrence, F. R.; Marshall, W. J.; Höke, H.; Jäckh, R. *Aniline. Ullmann's Encyclopedia of Industrial Chemistry*; Wiley-VCH Verlag GmbH & Co. **2000**.

Kumar, D.; Singh, S.; Khare, N. Plasmonic Ag nanoparticles decorated $NaNbO_3$ nanorods for efficient photoelectrochemical water splitting. *Int. J. Hydrogen Energ.* **2018**, *43*, 8198-8205.

(A) Lang, Q.; Yang, Y.; Zhu, Y.; Hu, W.; Jiang, W.; Zhong, S.; ... Bai, S. High-index facet engineering of PtCu cocatalysts for superior photocatalytic reduction of CO_2 to CH_4. *J. Mat. Chem. A.* **2017***, 5*, 6686-6694.

(B) Lang, Q.; Hu, W.; Zhou, P.; Huang, T.; Zhong, S.; Yang, L.; ...Bai, S. Twin defects engineered Pd cocatalyst on C_3N_4 nanosheets for enhanced photocatalytic performance in CO_2 reduction reaction. *Nanotech.* **2017**, *28*, 484003.

Lasia, A. Mechanism and kinetics of the hydrogen evolution reaction. *Int. J. Hydrogen Energ*. **2019**, *44*, 19484-19518.

Lee, K. J.; Kim, S.; Hong, W.; Park, H.; Jang, M. S.; Yu, K.; Choi, S. Y. Observation of Wavelength-Dependent Quantum plasmon tunneling with Varying the thickness of Graphene spacer. *Sci. Rep.* **2019**, *9*, 1-8.

Lei, Y., Zhao, G. F., & Zeng, Z. The electronic structure of silver clusters. *J. Nanosci. Nanotechnol.* **2010**. 10(8), 5483-5489.

Li, J.; Pan, Z.; Zhou, K. Enhanced photocatalytic oxygen evolution activity by formation of Ir@ IrO_x (OH) y core–shell heterostructure. *Nanotechnology*, **2018**, *29*, 405705.

Li, Y. H.; Li, C.; & Yang, H. G. Quantitative analysis of the PtO structure during photocatalytic water splitting by operando XAFS. *J. Mat. Chem. A* **2017**, *5*, 20631-20634.

Lin, C. A. J.; Lee, C. H.; Hsieh, J. T.; Wang, H. H.; Li, J. K.; Shen, J. L.; ... Chang, W. H. Synthesis of fluorescent metallic nanoclusters toward biomedical application: recent progress and present challenges. *J. Med. Biol. Eng*. **2009**, *29*, 276-283.

Linic, S.; Christopher, P.; & Ingram, D. B. Plasmonic-metal nanostructures for efficient conversion of solar to chemical energy. *Nat. Mater*. **2011,** *10*, 911-921.

Liu, H.; Wang, M.; Zhang, X.; Ma, J.; Lu, G. High efficient photocatalytic hydrogen evolution from formaldehyde over sensitized Ag@ Ag-Pd alloy catalyst under visible light irradiation. ***Appl. Catal. B***, **2018**, 237, 563-573.

Liu, L.; Zhang, X.; Yang, L.; Ren, L.; Wang, D.; Ye, J. Metal nanoparticles induced photocatalysis. *Natl. Sci. Rev.* **2017**, *4*, 761-780.

Li, L.; Zhao, S.; Joshi-Pangu, A.; Diane, M.; Biscoe, M. R. Stereospecific Pd-catalyzed cross-coupling reactions of secondary alkylboron nucleophiles and aryl chlorides. *J. Am. Chem. Soc.* **2014**, *136*, 14027-14030.

Li, X. H.; Baar, M.; Blechert, S.; Antonietti, M. Facilitating room-temperature Suzuki coupling reaction with light: Mott-Schottky photocatalyst for C-C coupling. *Sci. Rep.* **2013**, *3*, 1743.

Liu, Y.; Ai, K.; Cheng, X.; Huo, L.; Lu, L. Gold-nanocluster-based fluorescent sensors for highly sensitive and selective detection of cyanide in water. *Adv. Funct. Mater*. **2010**, *20*, 951-956.

Mallat, T.; Baiker, A. Oxidation of alcohols with molecular oxygen on solid catalysts. *Chem. Rev.* **2004**, *104*, 3037-3058.

Mei, B.; Pougin, A.; Strunk, J. Influence of photodeposited gold nanoparticles on the photocatalytic activity of titanate species in the reduction of CO_2 to hydrocarbons. *J. Catal.* **2013** *306*, 184-189.

Menger, F. M.; Lee, C. Synthetically useful oxidations at solid sodium permanganate surfaces. *Tetrahedron Lett.* **1981,** *22*, 1655-1656.

Metzger, J. O. Solvent-free organic syntheses. *Angew. Chem. Int. Ed.* **1998**, *37*, 2975-2978.

Moon, S. Y.; Song, H. C.; Gwag, E. H.; Nedrygailov, I. I.; Lee, C.; Kim, J. J.; ... Park, J. Y. Plasmonic hot carrier-driven oxygen evolution reaction on Au nanoparticles/TiO_2 nanotube arrays. *Nanoscale*, **2018**, *10*, 22180-22188.

Niishiro, R.; Tanaka, S.; Kudo, A. Hydrothermal-synthesized $SrTiO_3$ photocatalyst codoped with rhodium and antimony with visible-light response for sacrificial H_2 and O_2 evolution and application to overall water splitting. *Appl. Catal. B* **2014** *150*, 187-196.

Nitzan, A.; Brus, L. E.. Theoretical model for enhanced photochemistry on rough surfaces. *J. Chem. Phys.* **1981,** *75*, 2205-2214.

Ohno, T.; Higo, T.; Murakami, N.; Saito, H.; Zhang, Q.; Yang, Y.; Tsubota, T. Photocatalytic reduction of CO_2 over exposed-crystal-face-controlled TiO_2 nanorod having a brookite phase with co-catalyst loading. *Appl. Catal. B,* **2014,** *152*, 309-316.

Prati, L.; Martra, G. New gold catalysts for liquid phase oxidation. *Gold Bull.* **1999**, *32*, 96-101.

Raja, K. S.; Smith, Y. R.; Kondamudi, N.; Manivannan, A.; Misra, M.; Subramanian, V. R. CO_2 photoreduction in the liquid phase over Pd-supported on TiO_2 nanotube and bismuth titanate photocatalysts. *Electrochem. Solid-State Lett.* **2011**, *14*, F5

Scholl, J. A.; García-Etxarri, A.; Koh, A. L.; Dionne, J. A. Observation of quantum tunneling between two plasmonic nanoparticles. *Nano Lett.* **2013**, *13*, 564-569.

Sharma, S.; Kumar, D.; Khare, N. Plasmonic Ag nanoparticles decorated Bi_2S_3 nanorods and nanoflowers: their comparative assessment for photoelectrochemical water splitting. *Int. J. Hydrogen Energ.* **2019**, *44*, 3538-3552.

Shi, W.; Ma, C.; Wang, H.; Duan, D.; Sun, Z.; Yang, S. A sea cucumber-like nanoporous TiO_2 modified by bimetal PtAu through the dealloying for water splitting. *Int. J. Hydrogen Energ.* **2018**, *43*,18850-18862.

Sheng, W.; Myint, M.; Chen, J. G.; Yan, Y. Correlating the hydrogen evolution reaction activity in alkaline electrolytes with the hydrogen binding energy on monometallic surfaces. *Energy Environ. Sci.* **2019**, *6*, 1509-1512.

Shiraishi, Y.; shi, Y.; Imai, J.; Yasumoto, N.; Sakamoto, H.; Tanaka, S.; Ichikawa, S.; Hirai, T. Doping of Nb^{5+} species at the Au–TiO_2 Interface for Plasmonic Photocatalysis Enhancement. *Langmuir* **2019**, *35*, 5455-5462.

Shown, I.; Hsu, H. C.; Chang, Y. C.; Lin, C. H.; Roy, P. K.; Ganguly, A. Chen, K. H. Highly efficient visible light photocatalytic reduction of CO_2 to hydrocarbon fuels by Cu-nanoparticle decorated graphene oxide. *Nano Lett.* **2014**, *14*, 6097-6103.

Smith, J. G.; Faucheaux, J. A.; Jain, P. K. Plasmon resonances for solar energy harvesting: a mechanistic outlook. *Nano Today* **2015,** *10*, 67-80.

Song, H.; Meng, X.; Dao, T. D.; Zhou, W.; Liu, H.; Shi, L.; ... Ye, J. Light-enhanced carbon dioxide activation and conversion by effective plasmonic coupling effect of Pt and Au nanoparticles. *ACS Appl. Mater.* **2018**, *10*, 408-416.

Su, K. Y.; Chen, C. Y.; Wu, R. J. Preparation of Pd/TiO_2 nanowires for the photoreduction of CO_2 into renewable hydrocarbon fuels. *J Taiwan Inst Chem Eng*. **2019**, *96*, 409-418.

Tahir, M.; Tahir, B.; Amin, N. A. S. Gold-nanoparticle-modified TiO_2 nanowires for plasmon-enhanced photocatalytic CO_2 reduction with H_2 under visible light irradiation. *Appl. Surf. Sci.* **2015**, *356*, 1289-1299.

Tanaka, A.; Nishino, Y.; Sakaguchi, S.; Yoshikawa, T.; Imamura, K.; Hashimoto, K.; Kominami, H. Functionalization of a plasmonic Au/TiO_2 photocatalyst with an Ag co-catalyst for quantitative reduction of nitrobenzene to aniline in 2-propanol suspensions under irradiation of visible light. *ChemComm.* **2013**, *49*, 2551-2553.

Tian, J.; Li, J.; Wei, N.; Xu, X.; Cui, H.; Liu, H. Ru nanoparticles decorated TiO_2 nanobelts: A heterostructure towards enhanced photocatalytic activity and gas-phase selective oxidation of benzyl alcohol. *Ceram. Int.* **2016**, *42*, 1611-1617.

Tsukamoto, D.; Shiraishi, Y.; Sugano, Y.; Ichikawa, S.; Tanaka, S.; Hirai, T. Gold nanoparticles located at the interface of anatase/rutile TiO_2 particles as active plasmonic photocatalysts for aerobic oxidation. *J. Am. Chem. Soc.* **2012** *134*, 6309-6315.

Venkatesh, N.; Bhowmik, H.; Kuila, A. Metallic nanoparticle: a review. *Biomedical J. of Scientific and Technical Research,* **2018**, *4*, 3765-3775.

Wang, B.; Guo, X.; Jin, G.; Guo, X. Visible-light-enhanced photocatalytic Sonogashira reaction over silicon carbide supported Pd nanoparticles. *Catal. Commun.* **2017**, *98*, 81-84.

Wang, D.; Pierre, A.; Kibria, M. G.; Cui, K.; Han, X.; Bevan, K. H.; ... Mi, Z. Wafer-level photocatalytic water splitting on GaN nanowire arrays grown by molecular beam epitaxy. *Nano Lett.* **2011,** *11*, 2353-2357.

Wang, F.; Li, C.; Chen, H.; Jiang, R.; Sun, L. D.; Li, Q.; ... Yan, C. H. Plasmonic harvesting of light energy for Suzuki coupling reactions. *J. Am. Chem. Soc*. **2013,** *135*, 5588-5601.

Wang, M.; Zhen, W.; Tian, B.; Ma, J.; Lu, G. The inhibition of hydrogen and oxygen recombination reaction by halogen atoms on over-all water splitting over Pt-TiO_2 photocatalyst. *Appl. Catal. B* **2018**, *236*, 240-252.

Wang, M.; Zhang, S.; Li, M.; Han, A.; Zhu, X.; Ge, Q.; ... Wang, H. Facile synthesis of hierarchical flower-like Ag/Cu_2O and Au/Cu_2O nanostructures and enhanced catalytic performance in electrochemical reduction of CO_2. *Front. Chem. Sci. Eng*. **2020**, 1-11.

Wang, S.; Gao, Y.; Miao, S.; Liu, T.; Mu, L.; Li, R.; ... Li, C. Positioning the water oxidation reaction sites in plasmonic photocatalysts. *J. Am. Chem. Soc*. **2017**, *139*, 11771-11778.

Wang, W. N., An, W. J., Ramalingam, B., Mukherjee, S., Niedzwiedzki, D. M., Gangopadhyay, S., & Biswas, P. Size and structure matter: enhanced CO_2 photoreduction efficiency by size-resolved ultrafine Pt nanoparticles on TiO_2 single crystals. *JACS*. **2012,** 134(27), 11276-11281.

Wang, Y.; Ge, C. W.; Zou, Y. F.; Lu, R.; Zheng, K.; Zhang, T. F. Luo, L. B. Plasmonic Indium Nanoparticle-Induced High-Performance Photoswitch for Blue Light Detection. *Adv. Opt. Mater*. **2016**, *4*, 291-296.

Wang, Z. J.; Ghasimi, S.; Landfester, K.; Zhang, K. A. Photocatalytic Suzuki coupling reaction using conjugated microporous polymer with immobilized palladium nanoparticles under visible light. *Chem. Mater.* **2015**, *27*, 1921-1924.

Wiley, B. J.; Chen, Y.; McLellan, J. M.; Xiong, Y.; Li, Z. Y.; Ginger, D. Xia, Y. Synthesis and optical properties of silver nanobars and nanorice. *Nano Lett.* **2007**, *7*, 1032-1036.

Wisniak, Jaime. **2009**. "Jean Hellot. A pioneer of chemical technology. *Revista CENIC Ciencias Quimicas*. 40, 111-121.

Wu, L.; Duan, H.; Bai, P.; Bosman, M.; Yang, J. K.; Li, E. Fowler–Nordheim tunneling induced charge transfer plasmons between nearly touching nanoparticles. *ACS Nano* **2013,** *7*, 707-716.

Xiao, Q.; Jaatinen, E.; Zhu, H. Direct Photocatalysis for Organic Synthesis by Using Plasmonic-Metal Nanoparticles Irradiated with Visible Light. *Chem. Asian J.* **2014**, *9*, 3046-3064.

Xiao, Q.; Sarina, S.; Jaatinen, E.; Jia, J.; Arnold, D. P.; Liu, H.; Zhu, H. Efficient photocatalytic Suzuki cross-coupling reactions on Au–Pd alloy nanoparticles under visible light irradiation. *Green Chem.* **2014** *16*, 4272-4285.

Xiao, Q.; Sarina, S.; Waclawik, E. R.; Jia, J.; Chang, J.; Riches, J. D.; Zhu, H. Alloying gold with copper makes for a highly selective visible-light photocatalyst for the reduction of nitroaromatics to anilines. *ACS Catal*. **2016**, *6*, 1744-1753.

Xiao, S.; Liu, P.; Zhu, W.; Li, G.; Zhang, D.; Li, H. Copper nanowires: a substitute for noble metals to enhance photocatalytic H_2 generation. *Nano Lett.* **2015**, *15*, 4853-4858.

Xie, S., Wang, Y., Zhang, Q., Fan, W., Deng, W., & Wang, Y. Photocatalytic reduction of CO_2 with H_2O: significant enhancement of the activity of Pt–TiO_2 in CH_4 formation by addition of MgO. *Chem. Com*. **2013**, 49(24), 2451-2453.

Xing, J.; Chen, J. F.; Li, Y. H.; Yuan, W. T.; Zhou, Y.; Zheng, L. R.; Wang, Y. Stable isolated metal atoms as active sites for photocatalytic hydrogen evolution. *Chem. Eur. J.* **2014**, *20*, 2138-2144.

Xiong, Z., Lei, Z., Kuang, C. C., Chen, X., Gong, B., Zhao, Y. & Wu, J. C. Selective photocatalytic reduction of CO_2 into CH_4 over Pt-Cu_2O TiO_2 nanocrystals: The interaction between Pt and Cu2O cocatalysts. *Appl. Catal. B: Environ*. **2017**, 202, 695-703.

Xu, F.; Meng, K.; Cheng, B.; Yu, J.; Ho, W. Enhanced Photocatalytic Activity and Selectivity for CO_2 Reduction over a TiO_2 Nanofibre Mat Using Ag and MgO as Bi Cocatalyst. *ChemCatChem*. **2019,** *11*, 465-472.

Yang, C. T.; Wood, B. C.; Bhethanabotla, V. R.; Joseph, B. CO_2 adsorption on anatase TiO_2 (101) surfaces in the presence of subnanometer Ag/Pt clusters: implications for CO_2 photoreduction. The *J. Phys. Chem. C.* **2014**, *118*, 26236-26248.

Yang, C. T.; Wood, B. C.; Bhethanabotla, V. R.; Joseph, B. Electron injection study of photoexcitation effects on supported subnanometer Pt clusters for CO_2 photoreduction. *Phys. Chem. Chem. Phys.* **2018**, *20*, 15926-15938.

Zhang, L.; Can, M.; Ragsdale, S. W.; Armstrong, F. A. Fast and selective photoreduction of CO_2 to CO catalyzed by a complex of carbon monoxide dehydrogenase, TiO_2, and Ag nanoclusters. *ACS Catal.* **2018,** *8*, 2789-2795.

Zhang, Y.; Wang, X.; Dong, P.; Huang, Z.; Nie, X.; & Zhang, X. TiO_2 surfaces self-doped with Ag nanoparticles exhibit efficient CO_2 photoreduction under visible light. *RSC Adv.* **2018**, *8*, 15991-15998.

Zhou, Y.; Jin, C.; Li, Y.; & Shen, W. Dynamic behavior of metal nanoparticles for catalysis. *Nano Today* **2018**, *20*, 101-120.

Zhu, H.; Ke, X.; Yang, X.; Sarina, S.; Liu, H. Reduction of nitroaromatic compounds on supported gold nanoparticles by visible and ultraviolet light. *Angew. Chem. Int. Ed*. **2010**, *49*, 9657-9661.

Zhao, X.; Xie, J.; Liu, X.; Liu, X. Facilitating a high-performance photocatalyst for Suzuki reaction: Palladium nanoparticles immobilized on reduced graphene oxide-doped graphitic carbon nitride. *Appl. Organomet. Chem.* **2019**, *33*, e4623.